Angle-resolved photoemission of ordered Pb/Ni(111) surface phases

J. Libra, K. Veltruská, and V. Matolín*

Department of Electronics and Vacuum Physics, Faculty of Mathematics and Physics, Charles University, V Holešovičkách 2, 18000 Prague 8, Czech Republic

(Received 1 November 2006; revised manuscript received 7 March 2007; published 31 October 2007)

Pb/Ni(111) surface phases were investigated by angle-resolved photoemission spectroscopy. Annealing of the Pb/Ni(111) surface led to the formation of the $(\sqrt{3}\times\sqrt{3})R30°$ reconstruction characterized by a topmost layer consisting of a substitutional alloy. The transformation to the $(\sqrt{3}\times\sqrt{3})R30°$ structure was accompanied by a modification of the surface band structure confirming the formation of a new phase in the Ni(111) surface layer, characterized by a transformation from ferromagnetic to a nonmagnetic state. The modification was displayed as a disappearance of the $\boldsymbol{k}$-dependent exchange splitting in the topmost alloy layer that was observed on the clean Ni surface due to the energy difference between spin-up and spin-down states. Fermi surface mapping showed partial disappearance of splitting of bands crossing the Fermi level.

DOI: 10.1103/PhysRevB.76.165438 PACS number(s): 73.20.At, 73.61.At, 82.65.+r, 73.61.−r

I. INTRODUCTION

Ferromagnetism in transition metals is driven by atomiclike exchange and correlation effects in the partially filled *d*-electron shells that cannot be explained in the framework of a simple model of the electronic structure. Strong hybridization between *d* orbitals with *d*, *s*, and *p* orbitals of neighboring atoms is present. Nickel is an itinerant ferromagnet, which means that its magnetic moment is carried by the conduction band electrons. Ferromagnetic properties can be explained in terms of two separate sets of electrons, majority and minority, which split in two bands $d^{\uparrow}$ and $d^{\downarrow}$ separated by the exchange splitting energy E_{ex}. Because of a high density of *d* states at the Fermi level, magnetic properties are given mainly by the number of unoccupied states in the minority (upper) band.

Angle-resolved ultraviolet photoelectron spectroscopy (ARUPS) is an efficient tool for direct band mapping. In the case of nickel, ARUPS was used for an extended study of the minority and majority band structures.[1–3] On Ni(111), it was shown that ARUPS can provide information even on the top of the minority *d* band situated in the Boltzmann tail of the Fermi-Dirac distribution function above the Fermi level.[1] A study of the temperature dependent electronic structure of Ni(111) near the Fermi energy[3] showed that $E_{ex}\approx 270$ meV at 300 K decreased to zero above the Curie temperature due to $d^{\uparrow}$ and $d^{\downarrow}$ band collapse.

Hybridization of *d* orbitals of Ni with *s*,*p* orbitals of neighboring nonmagnetic atoms that could be considered as nonmagnetic spacers is responsible for dramatic changes of magnetic properties of Ni alloys and interfaces. Self-consistent calculations of magnetic and electronic properties of Ni surfaces and Ni-Cu alloys[4] showed that *s*,*p*-*d* hybridization was the main mechanism acting to suppress Ni magnetization. This effect is important in the case of nickel because the Ni *d* states are almost full, with the Fermi level close to the upper band edge. Metals such as Fe with more holes in the *d* band are not so sensitive to the shape and position of the *d*-band edge.

Lead–nickel is an excellent binary system permitting fundamental studies of *d*-*s*,*p* alloy surface magnetism. Lead is diamagnetic with a full *d* shell and forms, with nickel, well defined Pb-Ni(111) surface structures. Lead and nickel form surface phases, which have no corresponding bulk counterpart and which are limited to the first surface layer only. During the post few years, several studies have shown the structural variety of Pb/Ni(111) surface phases involving a strong modification of the effective radius of the Pb adsorbate atoms. Pb deposited on Ni(111) at 300 K formed (3×3) and (4×4) structures.[5–7] The (3×3) surface phase was observed for 1 ML (monolayer) of Pb atoms forming a close packed hexagonal structure with a Pb-Pb atom spacing of 3.74 Å corresponding to that of the bulk Pb(111) plane. A transition from the (3×3) to the (4×4) structure was observed after additional deposition of 0.2 ML. Annealing of the Pb-covered surface was found to give rise to a stable Ni(111)-$(\sqrt{3}\times\sqrt{3})R30°$-Pb surface phase[8] with Pb atoms incorporated into the first Ni(111) layer and with a Pb atom outward displacement of 0.2 Å. The formation of a Ni(111)-$(\sqrt{3}\times\sqrt{3})R30°$-Pb substitutional alloy was confirmed in Ref. 9 and the Pb atoms were suggested to be in the fcc sites. It was shown that in the alloy phase the Pb effective radius was 0.4 Å smaller than in bulk crystalline Pb. Tensor low-energy electron diffraction analysis of the Ni(111)-$(\sqrt{3}\times\sqrt{3})R30°$-Pb surface[10] confirmed earlier findings of a strong reduction in the effective radius, which was attributed to the influence of surface valence electron charge smoothing and an associated surface stress effect. The amplitude of the surface alloy rumpling was found to be 0.73 Å. In our previous work,[11] we have shown that the transformation to the $(\sqrt{3}\times\sqrt{3})R30°$ structure was accompanied by the appearance of a strong photoelectron diffraction effect, confirming the embedding of Pb atoms in the Ni(111) first surface layer. The Pb 5*d* core level shift indicated charge transfer from Pb to the surface, particularly for (4×4) and $(\sqrt{3}\times\sqrt{3})R30°$ structures.

In the present work, the formation of the Pb/Ni(111) surface alloy was investigated by means of ARUPS, resolving exchange-split bands in angular scans, and Fermi surface maps corresponding to the ferromagnetic state of Ni, as in Refs. 2 and 3. The exchange splitting E_{ex} was modified when the Pb-Ni(111) surface alloy was formed. It was explained in

terms of overlapping of a nonsplit surface Pb-Ni alloy *d* band and split subsurface Ni *d* band.

II. EXPERIMENT

The experiment was performed in an UHV chamber equipped with a 300 mm diameter multichannel hemispherical analyzer SPECS Phoibos 150, a dual Mg/Al x-ray source, helium UV lamp, Ar^+ ion source, and metal evaporation sources. The manipulator, controlled by stepping motors, allows heating of the sample and rotation in the azimuthal and polar directions. Ultraviolet photoelectron spectroscopy (UPS) spectra were acquired using He *I* radiation ($h\nu$=21.22 eV) and pass energy of 1 eV. The total resolution (analyzer+photons+natural line width) was determined by measuring the width of the Fermi level at room temperature. The measured width was 120 meV, whereas the intrinsic width of the Fermi level at this temperature is 100 meV; hence, the instrument resolution (analyzer +photons) is about 70 meV. For x-ray photoelectron spectroscopy (XPS), the Al $K\alpha$ line ($h\nu$=1486.6 eV) was used.

Angle-resolved XPS and UPS spectra were obtained by rotating the sample manipulator. The polar angle between the surface normal and the direction of outgoing (detected) electrons changed from 0 to 70°. The azimuthal rotation of −90° to 90°, together with the threefold crystal surface symmetry, made it possible to detect outgoing electrons in all crystallographically equivalent polar directions. The rotation of the manipulator stepping motors was controlled by software communicating with the analyzer control system. It permitted the acquisition of well-resolved angular intensity spectra, particularly in the case of UPS with a high crystal momentum resolution.

The nickel crystal was a disk of 10 mm diameter and 1.5 mm thickness, oriented to within 0.2° of the (111) plane. Cleaning was performed by cycles of sputtering and flashing to 970 K until no contamination was detected by XPS. The Pb metal was evaporated from a Knudsen cell onto the clean Ni(111) surface at 300 K.[11] Pb deposition for 6 min corresponded to the formation of a complete (3×3) structure, i.e., to the formation of one close packed monolayer of lead. This result was used to calibrate the evaporation time in terms of coverage.

III. RESULTS

The x-ray photoelectron diffraction (XPD) pattern presented in Fig. 1 was obtained by measuring the angular dependence of the Ni $2p_{3/2}$ intensity. It represents a typical picture of the fcc (111) surface local structure. The Pb/Ni(111) $(\sqrt{3}\times\sqrt{3})R30°$ structure gives practically identical patterns, confirming the formation of the surface substitutional alloy phase with a part of Ni scatterers substituted by Pb ones. The angle-resolved Pb core level spectra do not show any diffraction features, indicating that the Pb/Ni(111) system can be treated as a pure two-dimensional system with Pb atoms in the first layer only.

If E is the kinetic energy of the outgoing electron with respect to the vacuum level and ϑ the polar angle, the surface parallel wave vector of the initial state is

$$k_{\parallel} = \sqrt{2mE/\hbar^2}\,\sin\,\vartheta.$$

Thus, the initial state energies $E_i(\boldsymbol{k}_{\parallel})$ of an electron in a band structure can be determined directly from the experimental data. The kinetic energy was calculated using a sample work function Φ=5.22 eV.[3]

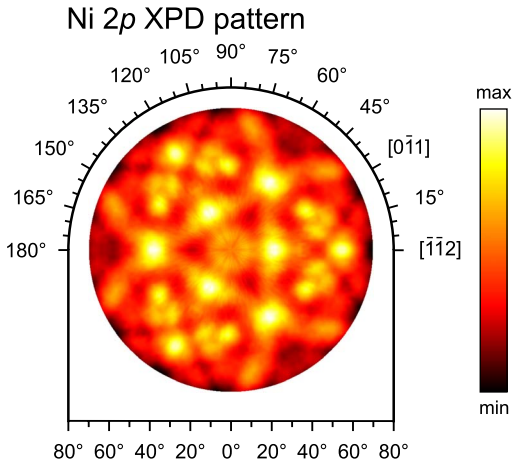

FIG. 1. (Color online) Angular distribution of the Ni $2p_{3/2}$ level intensity excited by $h\nu$=1486.6 eV. The XPD pattern is plotted on a color scale shown on the right. The same color representation is used in all subsequent figures.

By using our experimental system, we could clearly separate the states of different magnetic moments (parallel and antiparallel) as can be seen in the angular distribution curve plot of the clean Ni(111) surface presented in Fig. 2(a). This plot was obtained at a constant polar angle ϑ=44°, corresponding to $\boldsymbol{k}_{\parallel}$=1.42 Å^{-1} for the Fermi level, by scanning the azimuthal angle α relative to the $\bar{\Gamma}$-$\bar{M}'$ direction. Figure 2(a) shows that at certain points of the Brillouin zone, splitting of the *d* band is clearly visible.

The photoelectron intensity displayed in a linear gray scale gives a good three-dimensional picture of the band map; however, more detailed structure of the valence band can be visualized by plotting the energy distribution curves, i.e., the photoelectron spectra. The spectrum plotted in Fig. 2(a) at α=20° indicates two maxima: the lower at binding energy about 260 meV and the upper at 60 meV. Note that the minority band at this point of the surface Brillouin zone crosses the Fermi level. The photoemission spectrum is cut by the Fermi-Dirac distribution, and therefore the maximum of the photoemission spectrum (and so in this figure) is located at higher binding energy than the true center of the band.

In Fig. 2(b), of the Pb/Ni(111) $(\sqrt{3}\times\sqrt{3})R30°$ phase, the exchange splitting is less pronounced. The maximum of the majority band is shifted toward lower binding energy, and the intensity of the minority band is significantly lower. This could indicate an attenuation of the exchange splitting together with a shift of the whole band structure. Further insight brings the data measured by scanning of the polar angle

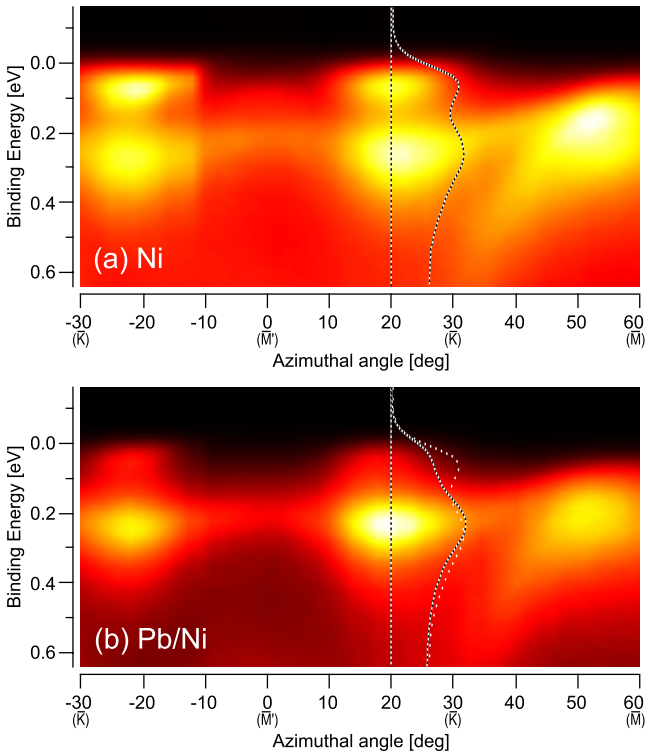

FIG. 2. (Color online) Angular distribution of photoemission spectra near the Fermi level acquired with varying azimuthal angle and fixed polar angle ϑ=44° from (a) clean Ni surface and (b) Pb-Ni alloy. Black-and-white-dotted lines show spectra for azimuthal angle ϕ=20°; white-dotted line in (b) is a spectrum from (a) for comparison.

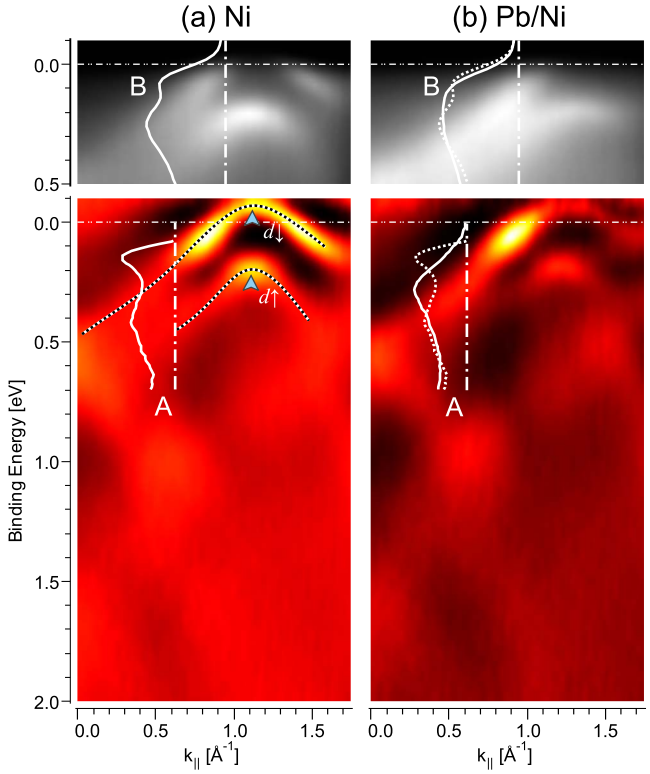

FIG. 3. (Color online) Angular distribution of photoemission spectra along the $\bar{\Gamma}$-$\bar{K}$ direction in the SBZ for (a) the clean Ni surface and (b) Pb-Ni alloy. Bottom panels show data after image processing; top panels show a part of the raw data near the Fermi level. Black-and-white dotted lines in (a) indicate split d bands. In (b), the d-band splitting is less pronounced. Spectrum "A" is a plot of image intensity below the dash-dotted line; the dotted line in (b) is a copy from (a) for comparison. Spectrum "B" shows raw data, where the decrease of the splitting is clearly visible.

and processed in order to visualize the states above the Fermi level.

Figure 3 displays the band structure of the Ni(111), Fig. 3(a), and Pb/Ni(111) $(\sqrt{3}\times\sqrt{3})R30°$ structure, Fig. 3(b), with $\boldsymbol{k}_{\parallel}$ along the $\bar{\Gamma}$-$\bar{K}$ direction in the (111) surface Brillouin zone. The data in Fig. 3 (bottom panels) are displayed by using image-processing routines in order to enhance the visibility and contrast of bands. Firstly, each row was normalized, i.e., divided by its average. This can compensate any intensity decrease due to the Fermi-Dirac cutoff. Secondly, the image contrast was enhanced by a high-pass filter. This filter removes low frequencies by subtracting slow intensity changes calculated by convoluting the image with two-dimensional Gaussian of width significantly higher than that of the features in the image. The raw (as measured) data are plotted in the upper panels of Fig. 3 for comparison.

In Fig. 3(a), the $d^{\downarrow}$ and $d^{\uparrow}$ band splitting of clean nickel is depicted by the dotted lines that were obtained by plotting the highest intensity in the band map. The top of the d band is found at approximately $\boldsymbol{k}_{\parallel}$=1.1 Å^{-1} and corresponding binding energies for $d^{\downarrow}$ and $d^{\uparrow}$ at about −60 and 200 meV, respectively [in Fig. 3(a) marked by blue arrows], which gives an E_{ex} value of 260 meV. The Ni(111) experimental band structure obtained in such a way corresponds rather well to the semiempirical band structure[12] along the $\bar{\Gamma}$-$\bar{K}$ line. There is also generally good agreement with the data in Ref. 3.

Figure 3(b) shows, with respect to Fig. 3(a), that the d-band splitting is significantly less pronounced in the case of the Pb-Ni(111) surface alloy formation. Two examples of the photoelectron spectra, A ($\boldsymbol{k}_{\parallel}$=0.6 Å^{-1}) and B ($\boldsymbol{k}_{\parallel}$=0.95 Å^{-1}, the point where the minority band crosses the Fermi level), show well the difference. Spectrum A is plotted by using the filtered data, and spectrum B shows the raw data.

At $\boldsymbol{k}_{\parallel}$=0.6 Å^{-1} (spectrum A), the collapsing band behavior is obvious because the $d^{\downarrow}$ and $d^{\uparrow}$ bands of clean nickel unite in one wide unresolved band. The behavior is discussed in more details in Sec. IV. The normalization used during the image processing could cause some distortion of band intensity; e.g., a bright spot in Fig. 3(b) clearly visible in processed data is not so distinct in unprocessed ones. Nevertheless, the d-band collapse is evident from the raw data presented in spectrum B, too. This spectrum shows a broad peak with unresolved maxima in Fig. 3(b).

In order to visualize Ni-Pb/Ni transitions at the Fermi level, we performed constant energy scanning that consists of setting of the energy window of the photoelectron analyzer to a small interval around a given binding energy. In Fig. 4, we present the plot obtained for the Ni(111) crystal

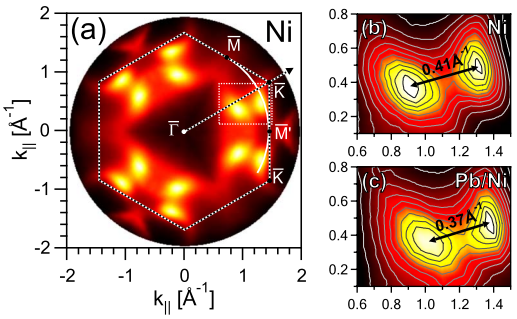

FIG. 4. (Color online) (a) Fermi surface map of the clean Ni surface. The plot is displayed as the area of the photoemission spectrum in the binding energy range of −0.02–0.02 eV as a function of $\boldsymbol{k}$. The dotted hexagon shows the surface Brillouin zone, the dotted line in the $\bar{\Gamma}$-$\bar{K}$ direction corresponds to the direction in which Fig. 3 was scanned, and the white arc corresponds to the azimuthal scan in Fig. 2. The detailed maps (b) and (c) display the region of the Fermi surface map marked in (a) by a white rectangle for clean Ni and the Pb/Ni surfaces, respectively.

taken in the binding energy interval −0.02–0.02 eV, i.e., corresponding to the Fermi surface (FS) scan. The surface Brillouin zone (SBZ) with symmetry points is included in the FS scan, and the $\bar{\Gamma}$-$\bar{K}$ direction is labeled by an arrow and corresponds to the angular distribution maps in Fig. 3. The white arc going from $\bar{M}$ to near $\bar{K}$ corresponds to the azimuthal scans in Fig. 2. A $\boldsymbol{k}_{\|}$ projection of the raw data is presented on a color scale, as in Fig. 1. The Fermi surface map of the clean surface shown in Fig. 4(a) is in relatively good agreement with the Fermi surface calculated for the Ni(111) surface in Ref. 2. The $d^{\downarrow}$ band crosses the Fermi level in two points, which can be seen in Fig. 3(a). These crossing points are displayed in Fig. 4 as bright double spots. Figures 4(b) and 4(c) show enlarged region of the double spot delimited by white rectangle in Fig. 4(a) for Ni(111) and Pb/Ni(111) $(\sqrt{3}\times\sqrt{3})R30°$ surfaces, respectively. The constant intensity contours plotted in Figs. 4(b) and 4(c) allow the determination of the crossing points with high precision. Figure 4(c) clearly reveals the crossing point's slightly approach with less pronounced minimum separating the maxima.

An essential feature of the Fermi surface plots in Fig. 4 is an empty triangular space around the $\bar{\Gamma}$ point. It corresponds well to the calculation for the He I excited Fermi surface of Ni(111) for *sp* minority electrons ($sp^{\downarrow}$), presented in Ref. 2. The Fermi energy contour corresponds to an intersection of the parabolic *sp* band $E_i(\boldsymbol{k}_{\|})$, exhibiting threefold symmetry of the fcc surface around $\bar{\Gamma}$. The transition from the pure Ni(111) surface to the Pb/Ni(111) alloy is observed as an extension of the Fermi surface contour due to the band boundary movement to lower energy and to its narrowing. It can be seen well if we slice the band by setting the analyzer to energies below the Fermi energy and perform constant energy surface scans. The results are presented in Fig. 5. The top pictures correspond to the pure Ni(111) surface and the bottom ones to the Pb/Ni(111) alloy. We can see that for clean nickel, the bottom of the gap is situated around

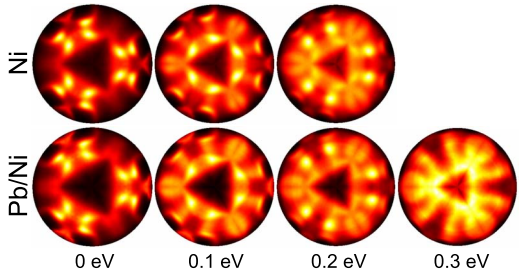

FIG. 5. (Color online) Closing of the triangular gap around the $\bar{\Gamma}$ point with increasing binding energy for the clean Ni surface and Pb-Ni alloy. Intensities are calculated from small intervals around the indicated binding energies.

0.25 eV, while for the alloy, it is at 0.35 eV. The existence of this gap can be predicted from the nickel band structure[12] because the (111) projected density of states of Ni shows a 0–0.3 eV gap in function of the exchange splitting value at the *L* point of the Brillouin zone. Thus, the difference between the prediction and measurement is relatively small.

IV. DISCUSSION

The band structure changes we observed showed that the formation of the Pb/Ni(111) $(\sqrt{3}\times\sqrt{3})R30°$ substitutional alloy was accompanied by noticeable changes of density of states in the proximity of the Fermi level. Both raw and filtered data in Figs. 2 and 3 reveal modifications of the *d*-band structure. The well-resolved $d^{\downarrow}$ and $d^{\uparrow}$ bands of the clean Ni(111) crystal give the E_{ex} value of 260 meV. The Pb/Ni(111) surface alloy formation causes a slight shift of the *d*-band maxima closer together, which gives an E_{ex} value of 230 meV, about 10% less than the value for clean nickel [see Fig. 3(b)]. The minimum separating the minority and majority bands in the valence band spectra is filled in due to the appearance of a new peak centered between the $d^{\downarrow}$ and $d^{\uparrow}$ bands. This behavior can be explained by a collapse of split spin-up and spin-down bands due to inclusion of diamagnetic Pb atoms into the nickel lattice in the first surface atomic layer. The formation of a broad unresolved *d* band can be explained in terms of overlapping of a surface Pb-Ni alloy *d* band, which is not exchange split, and a split subsurface Ni *d* band that was not, or less, affected by the surface lead atoms.

The magnetic properties are given by the number of unoccupied states in the minority (upper) band that is partially located above the Fermi energy. The points of the SBZ where the upper (minority) bands crossed the Fermi level are displayed as bright points in the Fermi surface scans (Fig. 4). When the splitting in the topmost alloy layer vanished, the crossing points approached with a less pronounced minimum separating the maxima. It could be again explained by the *d* band merging in the surface layer with a contribution of a nonsplit *d* band of the subsurface layers.

As a consequence of the surface alloy formation, the energy gap close to the $\bar{\Gamma}$ point expanded toward higher binding energy. This behavior was clearly observed even if one

can expect that the photoemission from the surface is superposed on the background of deeper Ni layers not affected by the surface alloy formation. It is obvious that the observed decrease of the exchange splitting can be explained by the transformation from the ferromagnetic Ni to the nonmagnetic Pb-Ni surface alloy. It means that replacing 1/3 of the surface Ni atoms by atoms of lead $[(\sqrt{3}\times\sqrt{3})R30°$ ordered structure] eliminates the surface magnetization. One can find a similarity with the temperature dependent experiment[2] where the exchange splitting vanished above the Curie temperature. In this experiment, all measurements were done at room temperature, so we were not confronted with the thermal effects affecting the energy bands.

The mechanism of the magnetic-nonmagnetic transition in the Pb-Ni surface layer can be explained in terms of a decrease of interatomic exchange coupling due to the introduction of lead spacers between Ni surface atoms. However, other mechanisms should be considered. The hybridization of s,p and d orbitals of Ni and Pb leads to a shift of the Ni d band to higher binding energy as can be seen from Fig. 5, as well as from a weaker bonding of CO on the surface.[11] This band shift leads to a decrease of the spin polarization of the itinerant d electrons ($n^{\uparrow}$-$n^{\downarrow}$ per atom). The shift to higher binding energy can explain why the collapsed band of the alloy is located at the same energy of 0.2 eV as the majority band of the clean Ni in Fig. 2. When the split bands merge, the d band should appear above the previous position of the majority band while the Ni and Pb orbital hybridizations push the nickel d band down.

V. CONCLUSIONS

In this work, we used ARUPS for a detailed investigation of the band structure. We have shown that by substituting 1/3 of the surface atoms of Ni(111) by lead, the exchange splitting partially vanishes and sp and d bands close to the Fermi level move to higher binding energy.

Two mechanisms can explain the exchange splitting disappearance: the ferromagnetic properties of Ni are suppressed when Ni atoms are adjacent to diamagnetic Pb atoms, which results in decreased exchange coupling, and the s,p-d hybridization shifts the Ni d band away from the Fermi energy and, consequently, the spin polarization and magnetic moment of surface Ni atoms decrease.

The effect of the surface alloy formation on magnetization is large only in the first Ni layer and seems to be negligible in deeper layers.

ACKNOWLEDGMENT

This work is a part of the Research Program No. MSM 0021620834 that is financed by the Ministry of Education of the Czech Republic.

*Corresponding author; Fax: +420 221 912 323; matolin@mbox.troja.mff.cuni.cz

[1] T. Greber, T. J. Kreutz, and J. Osterwalder, Phys. Rev. Lett. **79**, 4465 (1997).
[2] P. Aebi, T. J. Kreutz, J. Osterwalder, R. Fasel, P. Schwaller, and L. Schlapbach, Phys. Rev. Lett. **76**, 1150 (1996).
[3] T. J. Kreutz, T. Greber, P. Aebi, and J. Osterwalder, Phys. Rev. B **58**, 1300 (1998).
[4] J. Tersoff and L. M. Falicov, Phys. Rev. B **26**, 6186 (1982).
[5] K. Gürtler and K. Jacobi, Surf. Sci. **134**, 309 (1983).
[6] K. Gürtler and K. Jacobi, Surf. Sci. **152/153**, 272 (1985).
[7] K. Umezawa, A. Takahashi, T. Yumura, S. Nakanishi, and W. M. Gibson, Surf. Sci. **365**, 118 (1996).
[8] K. Umezawa, S. Nakanishi, T. Yumura, W. M. Gibson, M. Watanabe, Y. Kido, S. Yamamoto, Y. Aoki, and H. Naramoto, Phys. Rev. B **56**, 10585 (1997).
[9] D. Brown, P. D. Quinn, D. P. Woodruff, P. Bailey, and T. C. Q. Noakes, Phys. Rev. B **61**, 7706 (2000).
[10] P. D. Quinn, C. Bittencourt, and D. P. Woodruff, Phys. Rev. B **65**, 233404 (2002).
[11] V. Matolín, I. Matolínová, N. Tsud, S. Fabík, J. Libra, V. Dudr, V. Cháb, and K. C. Prince, Phys. Rev. B **74**, 075416 (2006).
[12] F. Weling and J. Callaway, Phys. Rev. B **26**, 710 (1982).